

A central role for TOR signalling in a yeast model for juvenile CLN3 disease

Michael E. Bond¹, Rachel Brown¹, Charalampos Rallis^{3,4}, Jürg Bähler^{3,4} and Sara E. Mole^{1,2,3,*}

¹MRC Laboratory for Molecular Cell Biology, University College London, London WC1E 6BT, UK.

²UCL Institute of Child Health, 30 Guilford Street, London WC1N 1EH, UK.

³Department of Genetics, Evolution and Environment, University College London, London WC1E 6BT, UK.

⁴Institute of Healthy Ageing, University College London, London WC1E 6BT, UK.

* Corresponding Author: Sara E. Mole, MRC Laboratory for Molecular Cell Biology, University College London; London WC1E 6BT, UK; Tel: +44 207 679 7257; Fax: +44 207 679 7805; E-mail: s.mole@ucl.ac.uk

ABSTRACT Yeasts provide an excellent genetically tractable eukaryotic system for investigating the function of genes in their biological context, and are especially relevant for those conserved genes that cause disease. We study the role of *btn1*, the orthologue of a human gene that underlies an early onset neurodegenerative disease (juvenile CLN3 disease, neuronal ceroid lipofuscinosis (NCLs) or Batten disease) in the fission yeast *Schizosaccharomyces pombe*. A global screen for genetic interactions with *btn1* highlighted a conserved key signalling hub in which multiple components functionally relate to this conserved disease gene. This signalling hub includes two major mitogen-activated protein kinase (MAPK) cascades, and centers on the Tor kinase complexes TORC1 and TORC2. We confirmed that yeast cells modelling CLN3 disease exhibit features consistent with dysfunction in the TORC pathways, and showed that modulating TORC function leads to a comprehensive rescue of defects in this yeast disease model. The same pathways may be novel targets in the development of therapies for the NCLs and related diseases.

INTRODUCTION

Yeasts have long been used as model systems to shed light on basic eukaryotic cell biology, and can provide a rapid and comprehensive route of investigation for genes of unknown function. This is particularly relevant for those genes that are conserved across diverse eukaryotic species and which can be presumed to play a fundamental biological role. A significant health challenge facing current research and drug development is the increasing incidence of age-related neurodegenerative disorders. Elucidating the mechanisms that underlie neurodegeneration is complex, particularly so in common age-related dementias that may have numerous contributing factors. There are, however, monogenic inherited neurodegenerative diseases that present a simpler alternative for investigation and real opportunities to determine these basic cellular changes, and some of the underlying genes are conserved even in yeasts. The genetic tractability of yeasts offers particular advantages to the challenges of understanding disease mechanisms in a relevant biological context and this knowledge

can inform therapeutic development for such conserved genetic diseases.

The neuronal ceroid lipofuscinoses (NCLs) are such a group of monogenic neurodegenerative disorders that generally affect children [1]. The most common of these is juvenile CLN3 disease [2]. This disease is characterised by progressive neuronal atrophy that causes visual failure, seizures and a progressive decline in cognitive and motor function. This disease is accompanied by cellular features characteristic of many neurodegenerative conditions [3, 4] that include the dysfunction of core cellular processes, such as reduced lysosomal and autophagic clearance [5, 6] and mitochondrial abnormalities [7]. Moreover, CLN3 disease also leads to specific cellular pathologies characteristic of more common dementias. These include the accumulation of lipofuscin [1], as observed in aged neurons [4], aberrant amyloid- β processing [5], a feature of Alzheimer's disease [8] and α -synuclein accumulation [9], a feature of Parkinson's disease [10].

Juvenile CLN3 disease is caused by mutations in a single gene (*CLN3*) [2], whose function is unknown but which is

doi: 10.15698/mic2015.12.241

Received originally: 06.08.2015;

in revised form: 12.10.2015,

Accepted 14.10.2015,

Published 11.11.2015.

Keywords: Batten disease, NCL, CLN3, *btn1*, Tor, TORC, *S. pombe*, yeast.

Abbreviations:

CWI - cell wall integrity,

NCLs - neuronal ceroid lipofuscinosis,

SAPK - stress-associated protein kinase,

SGA - synthetic genetic array,

WT - wild-type.

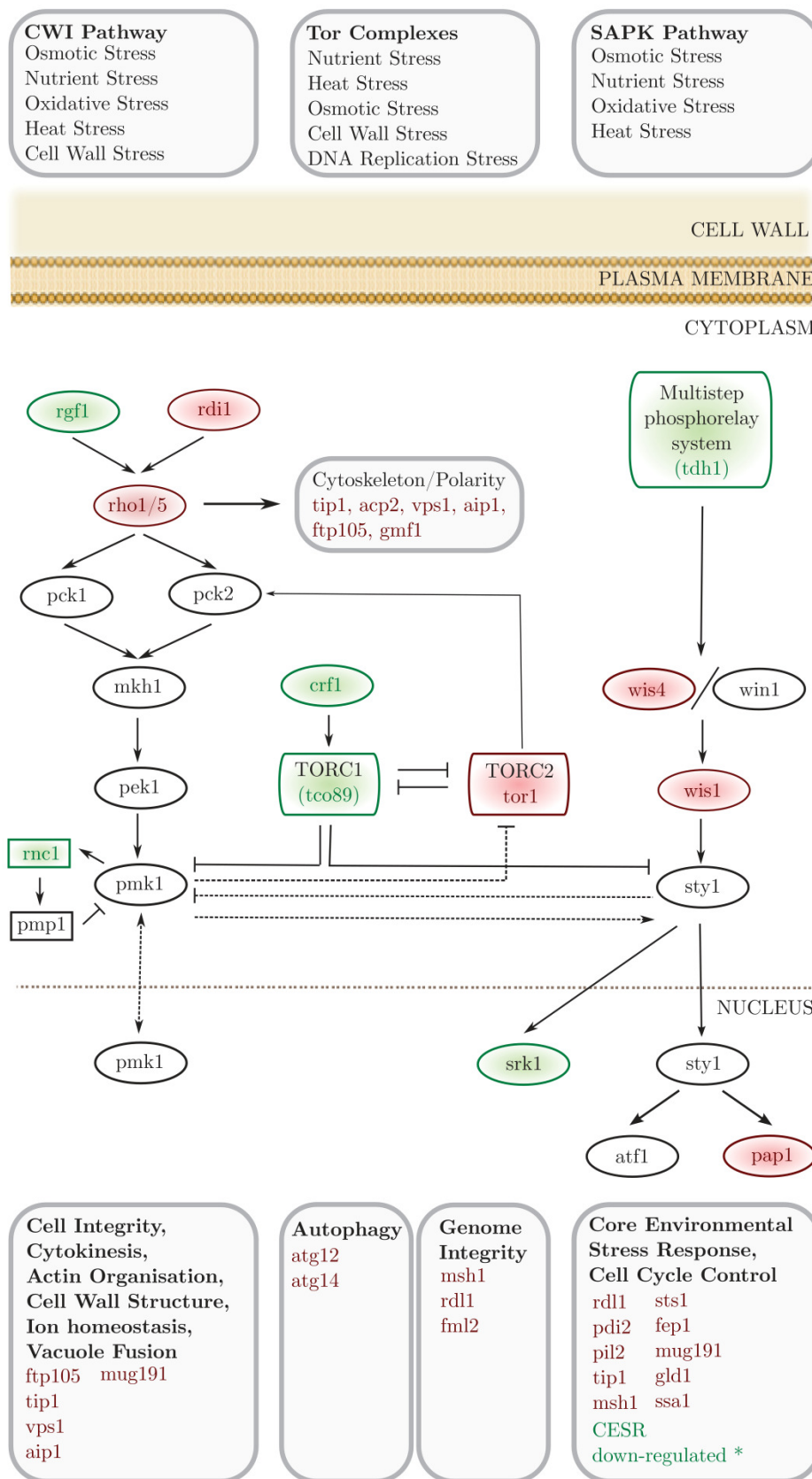


FIGURE 1: Synthetic genetic array (SGA) analysis of the genetic interactions of *btn1*. A schematic of the genes involved in stress responses that genetically interact with *btn1*. Genes in red were identified as negative interactors and those in green as positive. Grey genes are involved in these pathways but were not found to interact with *btn1*. * CESR refers to ‘core environmental stress response’ genes, a group of genes that respond to most environmental stressors as described by Chen *et al.* (2003) [76].

highly conserved across eukaryotic species [11]. As a consequence, this disease is relatively straightforward to reproduce in experimental systems and, given its similarity to more common dementias, such experimental models are ideal paradigms to study the basic cellular changes that occur in neurodegenerative diseases. The fission yeast *Schizosaccharomyces pombe* contains a single orthologue of *CLN3* (*btn1*) [11]. Work in this yeast has revealed a role for *btn1* in many cellular processes. Like patient cells, yeast lacking *btn1* (*btn1Δ*) have enlarged and less acidic vacuoles [12] and further work has supported roles for *btn1* in vacuolar homeostasis [13]. The ability of *btn1* modeling the most common CLN3 mutation (a 1 Kb deletion) to rescue these vacuolar defects found in the *btn1Δ* null strain has also revealed that this mutant allele retains some function, making juvenile CLN3 disease a mutation-specific disease rather than the consequence of a complete loss of function as originally assumed [14].

A host of further morphological defects exhibited in the *btn1Δ* strain support additional roles for *btn1* in cytokinesis [12] and the organisation of cell polarity [15]. Furthermore, *btn1Δ* cells also display cell wall defects [16]. Importantly, work in this model has expanded our understanding of the disease by revealing that *btn1* is involved in two independent pathways; one pH-dependent and one pH-independent, thus providing the first suggestion that Batten disease is more than a pH-related lysosome disorder [16]. Indeed, a comprehensive metabolomics approach has revealed that *btn1* is required for the regulation of glycolysis and amino acid homeostasis [17]. The involvement of *btn1* in numerous, apparently disparate, pathways may be a result of alterations at the Golgi apparatus, as the number, morphology, and location of this organelle are affected by its deletion [13]. Lastly, this model has been used successfully to model disease mutations in Btn1p, an effort that has provided valuable insight into their consequences on protein trafficking and function. It was found that equivalent CLN3 disease mutations in *btn1* affect the yeast phenotype in a way that can accurately predict the severity of disease, further establishing yeast as an accurate disease model despite its simplicity. Importantly, the observations reported in the fission yeast model have consistently been confirmed in mammalian systems [5, 18, 19]. Unfortunately however, despite these insights, the molecular processes that underlie cell death in this disease are poorly understood, the function of *CLN3* is unknown, and there remains a significant need for protective therapeutic targets.

A particular advantage of yeast model systems is the availability of genome-wide techniques. Synthetic genetic arrays (SGAs) have proved a particularly powerful means of exploring genetic interactions in yeast species [20]. This approach highlights genes involved in pathways parallel to, or converging with, the query gene. This provides information about functional relationships among genes, as well as processes that suppress the defects associated with a particular mutation. As they are hypothesis-free, SGAs are particularly valuable in the investigation of complex biological problems and those where gene function is unclear. These advantages are particularly relevant for neu-

rodegeneration in general, due to the complexity of the problem, and for juvenile CLN3 disease in particular, due to the lack of a clear gene function. SGAs have previously been employed in budding yeast to investigate mutant huntingtin and α -synuclein toxicity [21]. Such an approach can place the gene under investigation within its biological context and thereby uncover much-needed protective pathways for neurodegenerative disease.

We applied SGA analysis to identify pathways that are altered as a consequence of loss of function of *btn1* in an effort to better understand the molecular consequences of CLN3 disease, and to provide new candidate target pathways and processes for therapeutic development. A third of the genetic interactions that were identified centered on a set of conserved and connected signalling pathways. Manipulation of these pathways leads to a complete rescue of the pleiotropic array of *btn1Δ* phenotypes. This approach represents the most successful rescue of cellular dysfunction in any model for juvenile CLN3 disease to date.

RESULTS

Genome-wide analysis of genetic interactions with *btn1* reveals a central role for TOR kinases

We applied an SGA approach as an unbiased, genome-wide strategy to probe the interactions of a conserved neurodegenerative disease gene (*btn1*). We identified 331 positive interactors and 131 negative interactors of *btn1* (Table S1A and B). A large number of negative interactions ($n = 39$; 29.7%) mapped to a set of highly interconnected signalling processes, which center on the Tor kinase complexes TORC1 and TORC2 (Fig. 1). Core components of both complexes display genetic interactions with *btn1*; *tco89*, encoding a component of TORC1, was found to interact positively with *btn1*, while *tor1*, encoding the Tor kinase of TORC2, was found to interact negatively with *btn1*. Such a pattern suggests that TORC2 signalling is beneficial to the fitness of *btn1Δ* cells, whereas TORC1 signalling is detrimental, an observation that is in keeping with the idea that the two complexes play opposing roles and undergo mutual repression [22–24]. *btn1* was also found to negatively interact with genes encoding components of the connected cell wall integrity (CWI) and stress-associated protein kinase (SAPK) MAP kinase cascades, and a number of downstream stress regulated genes (Table S1A and B).

btn1Δ cells display features consistent with dysfunctional Tor signalling

The interaction of *btn1* with core TORC components, and the link to surrounding signalling processes, provides compelling evidence for the importance of Tor signalling in cells lacking *btn1*. To validate this observation, we investigated *btn1Δ* cells for features consistent with Tor dysfunction. Repression of TORC1 activity is required to mount a correct response to nitrogen limitation [24]. As loss of TORC1 activity was beneficial in cells lacking *btn1*, we hypothesised that these cells may display features consistent with dysregulation of TORC1 repression, and respond poorly to nitrogen limitation. To test this idea, we grew wild-type

and *btn1Δ* cells in minimal media, and minimal media lacking a nitrogen source, over 72 h. Viability was monitored at 24 h intervals using propidium iodide to label dead cells and calcofluor white to label the total cell population (Fig. 2A). Cells lacking *btn1* displayed a consistently lower viability in media lacking nitrogen, falling to $81.5 \pm 2.2\%$ after 24 h compared to $98.7 \pm 0.27\%$ in minimal media containing nitrogen ($P < 0.0015$, unpaired t test), and remaining lower throughout the time course. Wild-type cells displayed no change in viability when cultured in media lacking nitrogen.

TORC1 repression and TORC2 signalling is also required to mount a response to glucose limitation [25, 26]. Cells that are defective in TORC2 function do not respond appropriately to glucose limitation by reducing their cell length [26]. This is a relatively uncommon phenotype, with only *tor1* mutants and mutants in the Ca^{2+} /calmodulin-dependent-like gene *ssp1* known to display this phenotype [26, 27]. To test the ability of *btn1Δ* cells to adapt to conditions of limited glucose, we assessed both cell growth and the morphological response of these cells when grown

with an alternative carbon source (glycerol). Cells lacking *btn1* displayed a clear growth defect under these conditions (Fig. 2B). Wild-type and *btn1Δ* cells grown for 6 h in media containing either glucose or glycerol as a carbon source were stained with calcofluor white to visualise the cell wall. Cell elongation was determined using a measure of cell circularity and given a score of between 0 and 1, where 0 represents a perfectly round cell (Fig. 2C and D). Wild-type cells displayed a significant reduction in cell elongation upon growth in glycerol (0.25 ± 0.01 to 0.16 ± 0.01 , $P \leq 0.01$). Cells lacking *btn1*, however, displayed no significant change (0.32 ± 0.02 to 0.31 ± 0.02), consistent with a defect in their response to glucose limitation that is most likely linked to Tor1 function.

Lastly, TORC2 and the connected CWI pathway are also required for resistance to high temperature [26]. This temperature sensitivity of TORC2 and CWI pathway components is osmoremedial, i.e. it can be rescued by hypertonic growth media [28]. We confirmed the temperature sensitivity of *btn1Δ* cells, and that it can be rescued with 2M

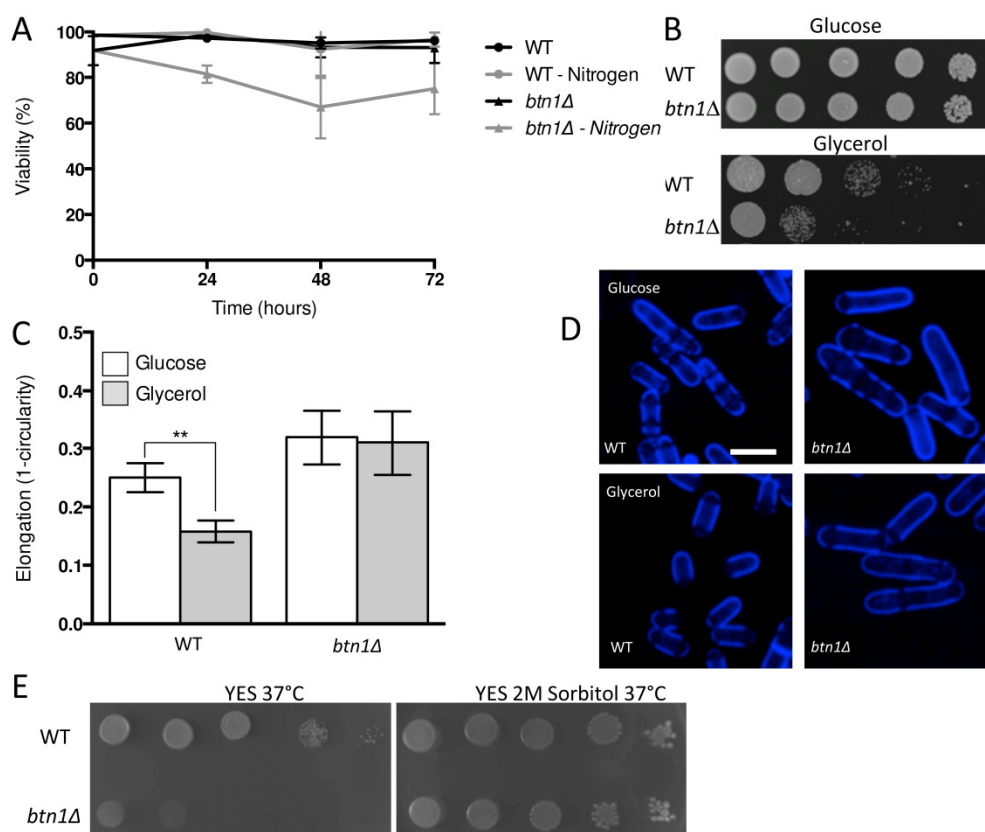


FIGURE 2: *btn1Δ* cells display features consistent with dysfunction in TOR signalling processes. (A) Cell viability upon nitrogen limitation was determined over periods of up to 72 hours in wild-type (WT) and *btn1Δ* cells, using the cell impermeable nucleotide stain propidium iodide to stain dead cells and calcofluor white to stain the total cell population. Cells were cultured in either MM or MM lacking a nitrogen source (NH_4Cl). 500 cells were scored for viability per data set, and data shown is a mean (\pm SEM) of 3 independent experiments. (B) WT cells and *btn1Δ* cells were serially diluted from a log-phase culture (1×10^6 cells/ml), and spotted onto plates containing either glucose or glycerol as a carbon source. Plates were then incubated at 30°C for 6 - 7 days to determine growth on fermentative and non-fermentative carbon sources. Images are representative of three independent experiments. (C) The morphological response of WT and *btn1Δ* cells to growth on glycerol was analysed following 6 hours in culture using a measure of cell elongation, on a scale of 0 to 1, where 0 represents a perfectly round cell ($1 - \frac{4\pi \text{ area}}{\text{perimeter}^2}$). Data shown is a mean (\pm SEM) of 5 independent experiments. Statistical significance between each condition was determined using a one-way ANOVA with a Tukey's multiple comparison post-test (** = $P < 0.01$). (D) Representative images of experiments as performed in (C) are shown. Scale bar represents $10 \mu\text{m}$. (E) WT and *btn1Δ* cells were also serially diluted from a log-phase culture (1×10^6 cells/ml) and spotted onto YES plates and YES plates containing 2M sorbitol. Plates were then incubated at 37°C for 3 - 4 days to determine the growth at high temperature and the influence of osmotic stabilisation. Images are representative of three independent experiments.

carbon sources. Images are representative of three independent experiments. (C) The morphological response of WT and *btn1Δ* cells to growth on glycerol was analysed following 6 hours in culture using a measure of cell elongation, on a scale of 0 to 1, where 0 represents a perfectly round cell ($1 - \frac{4\pi \text{ area}}{\text{perimeter}^2}$). Data shown is a mean (\pm SEM) of 5 independent experiments. Statistical significance between each condition was determined using a one-way ANOVA with a Tukey's multiple comparison post-test (** = $P < 0.01$). (D) Representative images of experiments as performed in (C) are shown. Scale bar represents $10 \mu\text{m}$. (E) WT and *btn1Δ* cells were also serially diluted from a log-phase culture (1×10^6 cells/ml) and spotted onto YES plates and YES plates containing 2M sorbitol. Plates were then incubated at 37°C for 3 - 4 days to determine the growth at high temperature and the influence of osmotic stabilisation. Images are representative of three independent experiments.

sorbitol (Fig. 2E), consistent with previous observations [16].

These data together indicate that cells lacking *btn1* display many features consistent with defects in Tor signalling

and function. Further, ectopic expression of *btn1* was able to rescue all these aspects of the mutant phenotype (Fig. S1A - D). Combined with the SGA results, these results suggest that Tor signalling is critical to the defects observed in

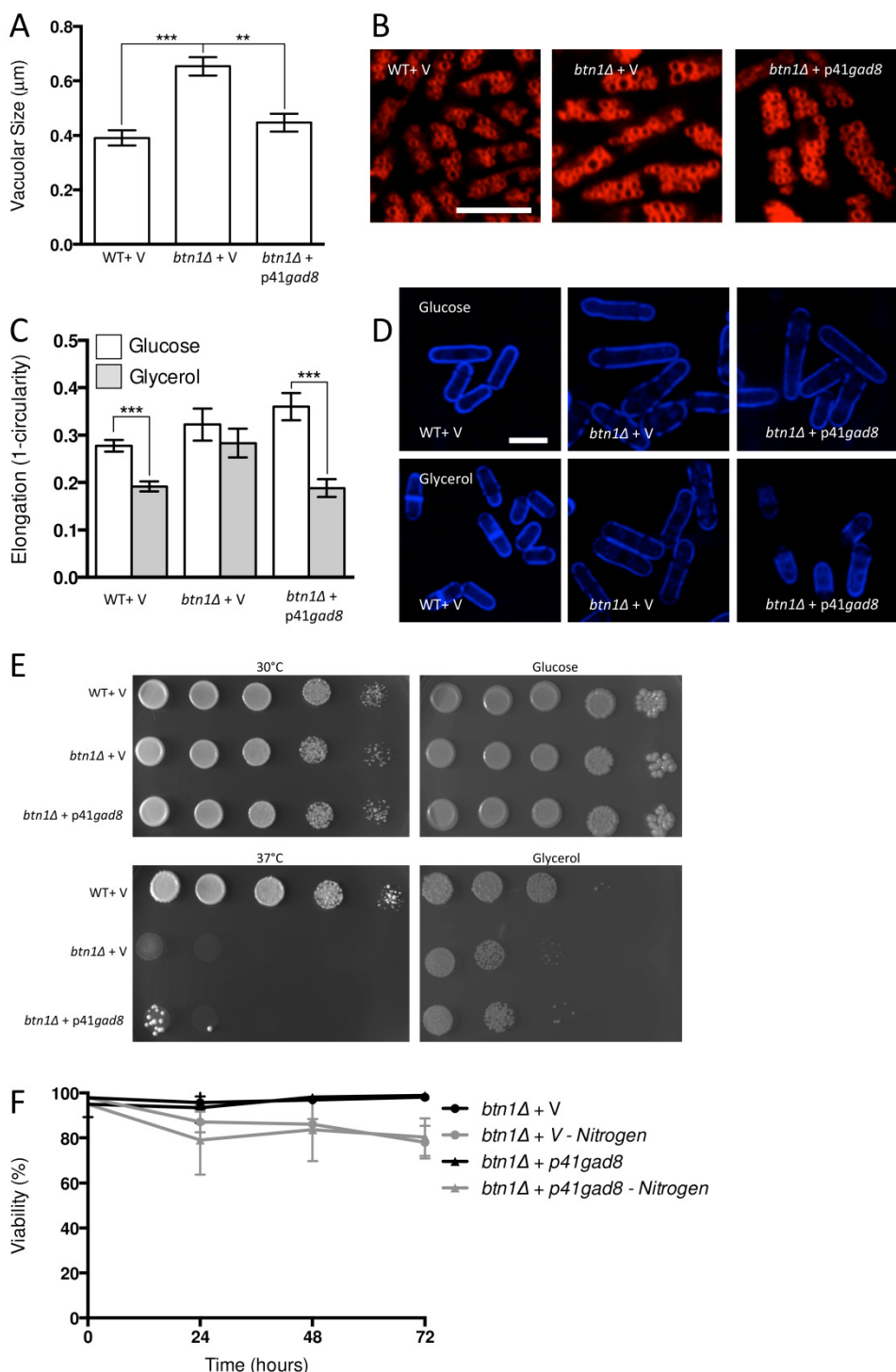


FIGURE 3: Increasing TORC2-dependent signalling rescues aspects of *btn1Δ* phenotype. (A) Cells lacking *btn1* were transformed with an expression vector containing *gad8*. Vacuole size was measured in these cells, in addition to WT and *btn1Δ* cells containing empty vector, following staining with the vital dye FM4-64. The diameter of 300 vacuoles was determined per data set, and data shown is a mean (± SEM) of 4 independent experiments. Statistical analysis was performed using a one-way ANOVA with a Tukey’s multiple comparison post-test (** = P < 0.01, *** = P < 0.001). (B) Representative images of experiments as performed in (A) are shown. Scale bar represents 10 μm. (C) The morphological response of these populations to growth on glycerol was analysed following 6 hours in culture using a measure of cell elongation, on a scale of 0 to 1, where 0 represents a perfectly round cell ($1 - \frac{4 \pi \text{ area}}{\text{perimeter}^2}$). Data shown is a mean (± SEM) of 5 independent experiments. Statistical significance between each condition was determined using a one-way ANOVA with a Tukey’s multiple comparison post-test (** = P < 0.001). (D) Representative images of experiments as performed in (C) are shown. Scale bar represents 10 μm. (E) These cells were serially diluted from a log-phase culture (1×10^6 cells/ml) and spotted onto YES plates. Plates were then incubated at 30°C or 37°C for 3 - 4 days to determine growth at high temperature.

They were also spotted onto plates containing either glucose or glycerol as a carbon source. Plates were then incubated at 30°C for 6 - 7 days to determine growth under non-fermentative conditions. Images are representative of three independent experiments. (F) Viability upon nitrogen limitation was determined over periods of up to 72 hours in these cell populations, using propidium iodide to stain dead cells and calcofluor white to stain all cells. Cells were cultured in either MM or MM lacking a nitrogen source (NH₄Cl). 500 cells were scored for viability per data set, and data shown is a mean (± SEM) of 3 independent experiments.

btn1Δ cells.

TORC2 and CWI pathway: modulating distinct signalling nodes elicit different levels of correction in *btn1Δ* cells

Given the negative genetic interaction between *btn1* and *tor1*, increasing TORC2 activity could alleviate aspects of the *btn1Δ* phenotype. We initially explored this approach through overexpression of the downstream kinase *Gad8*, which is a multicopy suppressor of aspects of the loss of TORC2 [29]. A key phenotype in cells lacking *btn1*, and one that is strongly linked to the phenotype of CLN3 disease, is a change in vacuole homeostasis [12]. One of the clearest manifestations of this feature in *btn1Δ* cells is an increase in vacuole size [12]. We investigated vacuole size in wild-type and *btn1Δ* cells containing empty vector alone (as a control), as well as *btn1Δ* cells expressing *gad8* from the *nmt1* promoter of the pREP41 plasmid (Fig. 3A and B). Consistent with previous reports, *btn1Δ* cells exhibited significantly larger vacuoles than wild-type cells ($0.65 \pm 0.03 \mu\text{m}$ compared to $0.39 \pm 0.01 \mu\text{m}$, $P \leq 0.001$). The overexpression of *gad8* in *btn1Δ* cells significantly rescued vacuole size ($0.40 \pm 0.03 \mu\text{m}$) ($P \leq 0.01$), restoring them to near that of wild-type. These data provide the first indication that increasing TORC2 function significantly rescues a disease-relevant phenotype of *btn1Δ* cells.

As discussed above, the ability of cells to respond to glucose-limitation with a change in cell size requires TORC2 function [26]. To investigate whether the inability of *btn1Δ* cells to undergo this morphological response can be rescued by increasing TORC2 pathway activity, we assessed the elongation of *btn1Δ* cells overexpressing *gad8* following growth for 6 hours in media containing either glucose or glycerol as a carbon source (Fig. 3C and D). Wild-type and *btn1Δ* cells containing empty vector alone displayed comparable responses to cells without vector (WT glucose - 0.28 ± 0.01 , WT glycerol - 0.19 ± 0.01 , $P \leq 0.001$; *btn1Δ* glucose - 0.32 ± 0.02 , *btn1Δ* glycerol - 0.28 ± 0.01 , ns). The overexpression of *gad8* was able to significantly rescue this morphological response, despite these cells being elongated under growth in glucose (glucose - 0.36 ± 0.01 , glycerol - 0.19 ± 0.01 , $P \leq 0.001$).

Despite this rescue, expression of *gad8* was unable to significantly rescue the growth of *btn1Δ* cells on glycerol or at high temperature, suggesting that the ability of these cells to adapt to heat and nutrient stress is still impaired (Fig. 3E). Similarly, expression of *gad8* was unable to rescue the viability of *btn1Δ* cells grown in the absence of a nitrogen source (Fig. 3F).

Given that the phenotypes not rescued by increasing TORC2 activity were linked to stress and nutrient adaptation, we reasoned that modulating processes more closely linked to the CWI pathway might be more effective in correcting these phenotypes. These processes seem particularly relevant in this instance, as this pathway is known to respond to both heat and glucose limitation. In particular, mutants of the *pmk1* MAP kinase, like *btn1Δ* mutants, display a partial growth defect on glycerol. Further, this pathway is required for proper activation of *Sty1* (the MAP kinase of the SAPK pathway) under glucose-limitation, inte-

grating these processes with further identified *btn1* interactors [30].

To increase CWI activity, we chose to increase Rho GTPase levels in these cells, which represent a key hub in CWI pathway regulation, by overexpressing the *btn1* interactor *rho5* and its essential paralogue *rho1*. Overexpression of *rho1* significantly decreased vacuole size in *btn1Δ* cells ($P \leq 0.001$) to near that of wild-type cells containing empty vector alone (WT - $0.30 \pm 0.02 \mu\text{m}$, *btn1Δ* - $0.47 \pm 0.04 \mu\text{m}$, *btn1Δ* with p41*rho1* - $0.32 \pm 0.01 \mu\text{m}$) (Fig. 4A and B). The overexpression of *rho5* led to an over-correction of this phenotype ($0.19 \pm 0.01 \mu\text{m}$), producing vacuoles significantly smaller than those of *btn1Δ* cells ($P \leq 0.001$) and wild-type cells containing vector alone ($P \leq 0.05$). Consistent with these observations, over-expression of *pmp1*, which inhibits the activity of *pmk1* [31], caused an increase in vacuole size in *btn1Δ* cells (*btn1Δ* with p41*pmp1* - $0.80 \pm 0.08 \mu\text{m}$ vs *btn1Δ* - $0.52 \pm 0.04 \mu\text{m}$, $P \leq 0.01$) but not in wild-type cells (WT with p41*pmp1* - $0.24 \pm 0.01 \mu\text{m}$ vs WT - 0.23 ± 0.02 , ns) (Fig. 4C). Such data indicate that increasing CWI pathway activity is able to correct the vacuole defect of *btn1Δ* cells, and directly inhibiting this pathway exacerbates the vacuole defect. The over-correction by *rho5* could indicate a strong dose-dependence in this particular rescue. Indeed, previous work has demonstrated such dose dependence in the relationship between *btn1* and vacuole size [12].

We next investigated whether the Rho GTPases were able to rescue the morphological response of these cells to glycerol, as seen with *gad8*. We looked just at *rho1* in this case, as *rho5* overexpression has a pronounced effect on cell shape and septation [32], making morphological comparisons difficult (Fig. S2). Overexpression of *rho1* elicited a rescue of this response, with cells displaying a significant reduction in cell elongation when grown in glycerol containing media (0.28 ± 0.02 to 0.16 ± 0.01 , $P \leq 0.01$) (Fig. 4D and E).

Further to a rescue of the morphological response to glycerol, both *rho1* and *rho5* were able to correct the growth defect of *btn1Δ* cells on glycerol as a carbon source. In addition, *rho1* was able to rescue the temperature sensitivity phenotype of these cells (Fig. 4F). The overexpression of *rho5* did not correct this phenotype, although, given the link between heat-sensitivity and septation defects in *btn1Δ* cells [15] and the enhanced septation defect of cells overexpressing *rho5* (Fig. S2), this is not wholly unexpected.

In addition to these phenotypes, overexpression of *rho1* and *rho5* rescued the viability of *btn1Δ* cells when grown in the absence of a nitrogen source, with viability remaining higher than 95% throughout the course of the experiment (Fig. 4G). These data provide evidence for a profound positive interaction between CWI pathway signalling and *btn1*, indicating that such processes are intimately linked with the defects that occur in *btn1Δ* cells.

Reducing TORC1 activity corrects defects in *btn1Δ* cells

TORC1 activity is a key signal of a favourable environment, promoting proliferation and suppressing stress-responsive

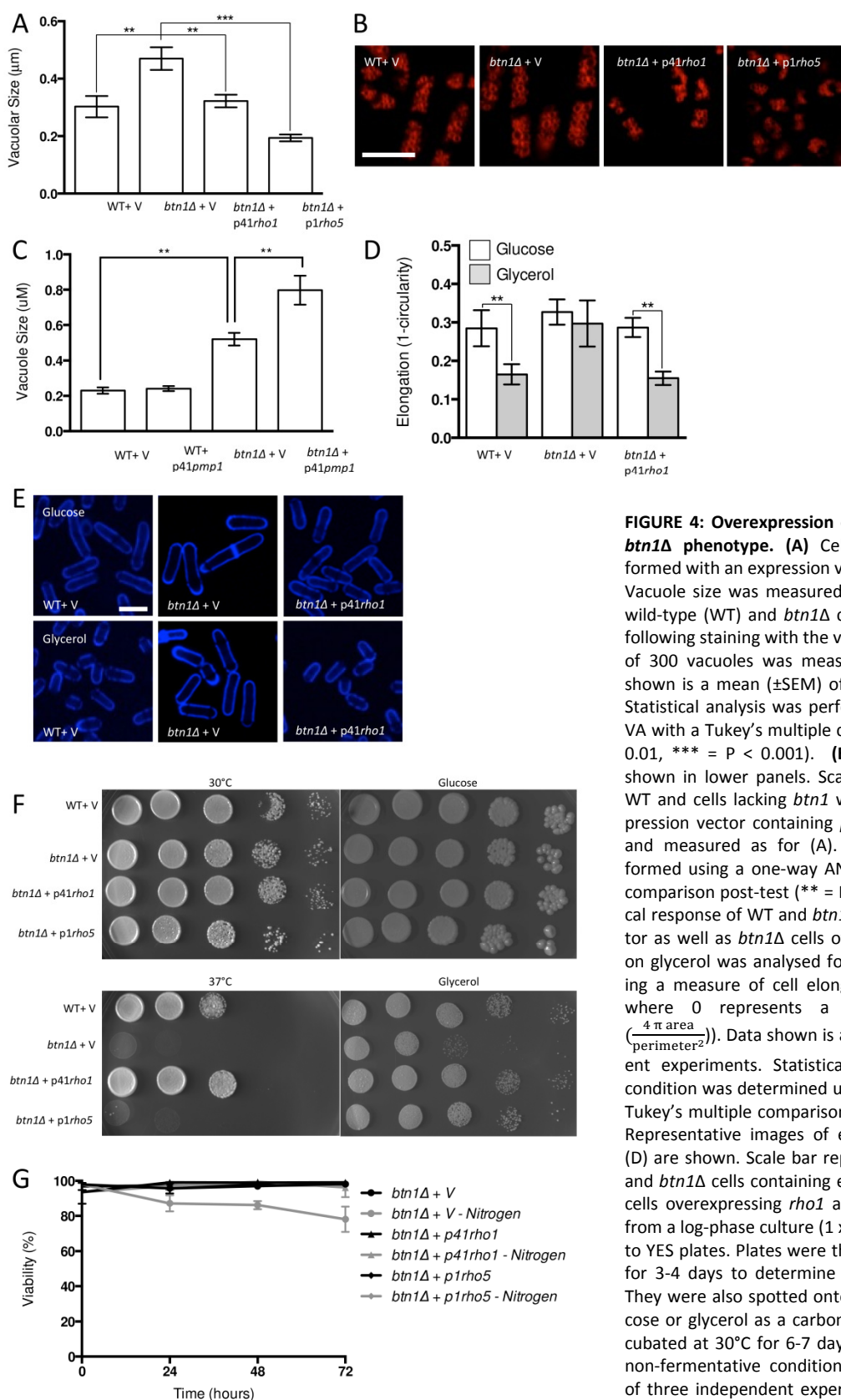


FIGURE 4: Overexpression of Rho rescues all aspects of *btn1Δ* phenotype. (A) Cells lacking *btn1* were transformed with an expression vector containing *rho1* or *rho5*. Vacuole size was measured in these cells, in addition to wild-type (WT) and *btn1Δ* cells containing empty vector, following staining with the vital dye FM4-64. The diameter of 300 vacuoles was measured per data set, and data shown is a mean (\pm SEM) of 4 independent experiments. Statistical analysis was performed using a one-way ANOVA with a Tukey's multiple comparison post-test (** = $P < 0.01$, *** = $P < 0.001$). (B) Representative images are shown in lower panels. Scale bar represents 10 μ m. (C) WT and cells lacking *btn1* were transformed with an expression vector containing *pmp1*. Vacuoles were stained and measured as for (A). Statistical analysis was performed using a one-way ANOVA with a Tukey's multiple comparison post-test (** = $P < 0.01$). (D) The morphological response of WT and *btn1Δ* cells containing empty vector as well as *btn1Δ* cells overexpressing *rho1* to growth on glycerol was analysed following 6 hours in culture using a measure of cell elongation, on a scale of 0 to 1, where 0 represents a perfectly round cell ($1 - \frac{4\pi \text{ area}}{\text{perimeter}^2}$). Data shown is a mean (\pm SEM) of 5 independent experiments. Statistical significance between each condition was determined using a one-way ANOVA with a Tukey's multiple comparison post-test (** = $P < 0.01$). (E) Representative images of experiments as performed in (D) are shown. Scale bar represents 10 μ m. (F) Wild-type and *btn1Δ* cells containing empty vector as well as *btn1Δ* cells overexpressing *rho1* and *rho5* were serially diluted from a log-phase culture (1×10^6 cells/ml) and spotted onto YES plates. Plates were then incubated at 30°C or 37°C for 3-4 days to determine growth at high temperature. They were also spotted onto plates containing either glucose or glycerol as a carbon source. Plates were then incubated at 30°C for 6-7 days to determine growth under non-fermentative conditions. Images are representative of three independent experiments. (G) Viability upon nitrogen limitation was determined over periods of up to 72

hours in these cell populations, using propidium iodide to stain dead cells and calcofluor white to stain all cells. Cells were cultured in either MM or MM lacking a nitrogen source (NH_4Cl). 500 cells were scored for viability per data set, and data shown is a mean (\pm SEM) of 3 independent experiments.

processes [24]. As a consequence, it is antagonistic to many of the processes explored in this study that improved the *btn1Δ* phenotype. TORC1 represses TORC2 function [23], and negatively regulates Sty1 [33], which displays extensive cross-talk with the CWI pathway [30]. This relationship is highlighted by the fact that the core TORC1 component gene *tco89* is a positive interactor of *btn1*.

In order to test whether repression of TORC1 activity could rescue the phenotypes of *btn1Δ* cells, we first overexpressed a dominant-negative form of the upstream activator of TORC1, Rhb1 (*rhb1^{D60K}*) [34]. Upon overexpression of dominant-negative *rhb1* (*dnrhb1*) in *btn1Δ* cells, we observed a significant reduction ($P \leq 0.001$) in vacuole size compared to *btn1Δ* cells containing vector alone (*btn1Δ* with *p41dnrhb1* - $0.40 \pm 0.04 \mu\text{m}$, *btn1Δ* with empty vector

- $0.65 \pm 0.03 \mu\text{m}$) (Fig. 5A and B). This result was comparable to the vacuole size of wild-type cells ($0.39 \pm 0.01 \mu\text{m}$), indicating a rescue of vacuole morphology upon repression of TORC1 activity.

We next investigated the ability of TORC1 repression to rescue the nutrient-sensing defects of cells lacking *btn1*. The overexpression of *dnrhb1* led to a significant rescue of the morphological response of these cells to glucose-limitation, following 6 hours growth in glycerol as a carbon source (Fig. 5C and D). Cell elongation fell from 0.29 ± 0.02 to 0.18 ± 0.01 when grown in glycerol as opposed to glucose, a response comparable to that observed in wild-type cells (glucose - 0.28 ± 0.01 , glycerol - 0.19 ± 0.01). This also corresponded to a rescue of the growth defect of these cells on glycerol (Fig. 5E). Further to the glycerol growth

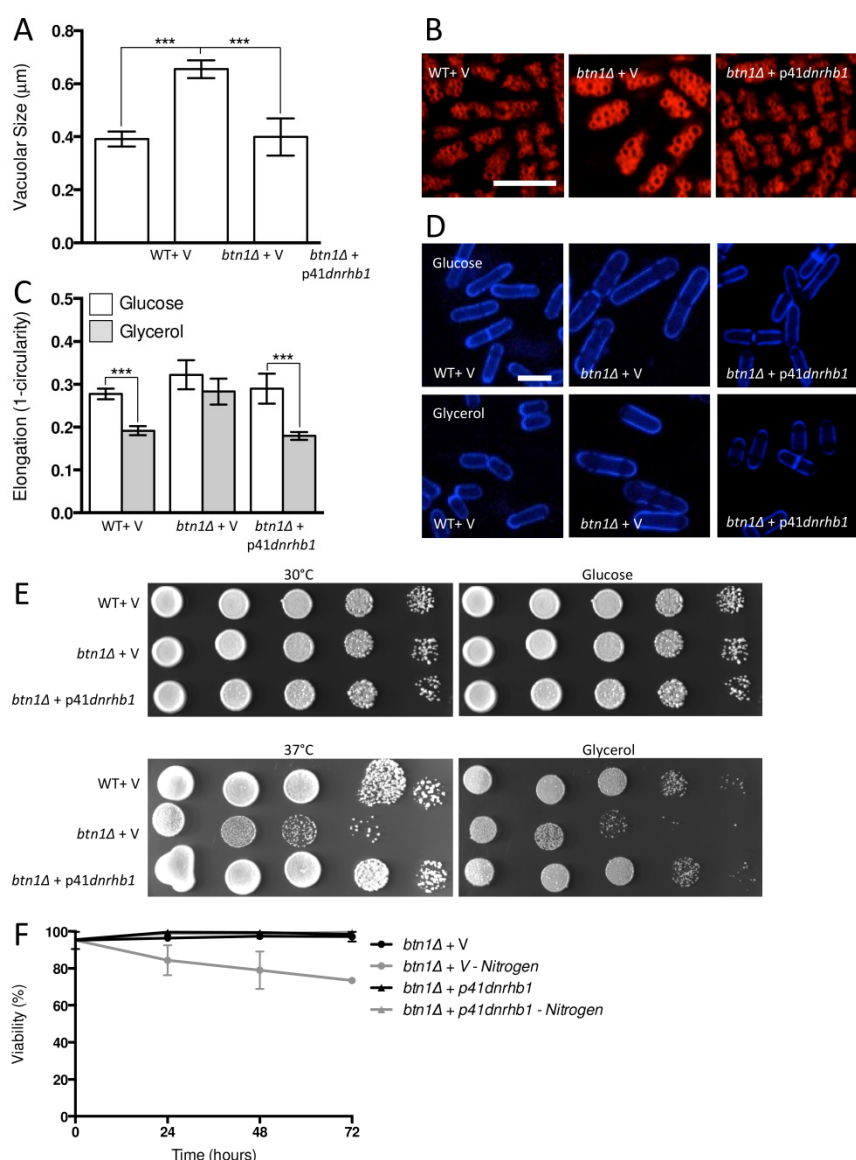


FIGURE 5: Inhibiting TORC1 function rescues the defects in *btn1Δ* cells.

(A) Cells lacking *btn1* were transformed with an expression vector containing a dominant-negative form of *rhb1* (*dnrhb1*). Vacuole size was measured in these cells, in addition to wild-type (WT) and *btn1Δ* cells containing empty vector, following staining with the vital dye FM4-64. The diameter of 300 vacuoles was measured per data set, and data shown is a mean (\pm SEM) of 4 independent experiments. Statistical analysis was performed using a one-way ANOVA with a Tukey's multiple comparison post-test (***) = $P < 0.001$). (B) Representative images of experiments as performed in (A) shown. Scale bar represents 10 μm . (C) The morphological response of these populations to growth on glycerol was analysed following 6 hours in culture using a measure of cell elongation, on a scale of 0 to 1, where 0 represents a perfectly round cell ($1 - \frac{4\pi \text{ area}}{\text{perimeter}^2}$). Data shown is a mean (\pm SEM) of 5 independent experiments. Statistical significance between each condition was determined using a one-way ANOVA with a Tukey's multiple comparison post-test (***) = $P < 0.001$. (D) Representative images of experiments as performed in (C) shown. Scale bar represents 10 μm . (E) These cells were serially diluted from a log-phase culture (1×10^6 cells/ml) and spotted onto YES plates. Plates were then incubated at 30°C or 37°C for 3-4 days to determine growth at high temperature. They were also spotted onto plates containing either glucose or glycerol as a carbon source. Plates were then incubated at 30°C for 6-7 days to determine growth under non-fermentative conditions. Images are representative of three independent experiments. (F) Viability upon nitrogen limitation was determined over periods of up to 72 hours in these cell populations,

using propidium iodide to stain dead cells and calcofluor white to stain all cells. Cells were cultured in either MM or MM lacking a nitrogen source (NH_4Cl). 500 cells were scored for viability per data set, and data shown is a mean (\pm SEM) of 3 independent experiments. Scale bar represents 10 μm .

defect, *dnrhb1* overexpression also rescued the heat sensitivity of *btn1Δ* cells (Fig. 5E). Finally, this construct was also able to elicit a complete rescue of viability under nitrogen limiting conditions, with viability remaining above 95% throughout the course of the experiment (Fig. 5F).

Given the substantial rescue of *btn1Δ* cells by *dnrhb1*-mediated activation of TORC1, we wanted to confirm the interaction between *btn1* and TORC1 by another means. We chose to use two pharmacological inhibitors of TORC1, rapamycin (allosteric) and caffeine (competitive inhibitor of ATP binding) [35]. TORC1 antagonism leads to cell rounding, a response that mimics the morphological change ordinarily exhibited by wild-type cells in response to nitrogen and amino acid starvation. Therefore, we examined the effect of TORC1 antagonism on cell rounding [36] and on vacuole size, heat sensitivity, and growth in glycerol. As expected, wild-type cells displayed a significant reduction in cell elongation upon rapamycin treatment for 6 hours (0.26 ± 0.02 to 0.15 ± 0.01 , $P \leq 0.01$) (Fig. 6A and B). This reduction in cell elongation did not change further upon exposure to

both rapamycin and caffeine [35]. Cells lacking *btn1*, however, did not respond to rapamycin, displaying only a slight morphological change (0.30 ± 0.01 to 0.25 ± 0.02) that was slightly enhanced by the addition of caffeine and rapamycin, but again not significantly (0.22 ± 0.03) (Fig. 6A and B). The addition of caffeine and rapamycin to wild-type cells did not significantly affect vacuole size (vehicle - $0.37 \pm 0.05 \mu\text{m}$, rapamycin - 0.31 ± 0.03 , caffeine and rapamycin 0.24 ± 0.01) (Fig. 6C and D). Rapamycin alone had no effect on the vacuole size of cells lacking *btn1*, but, in contrast, a combination of caffeine and rapamycin significantly ($P \leq 0.001$) reduced vacuole size (vehicle - $0.58 \pm 0.03 \mu\text{m}$, rapamycin - 0.55 ± 0.04 , caffeine and rapamycin 0.30 ± 0.02) (Fig. 6C and D). Further, treatment with rapamycin alone elicited a rescue of both the heat sensitivity defect and glycerol growth defect of cells lacking *btn1* (Fig. 6E). The ability of these pharmacological treatments to rescue the defects in vacuole size, heat sensitivity and growth in glycerol of *btn1Δ* cells appears to be closely linked to their ability to target TORC1 signalling itself, as opposed to changes

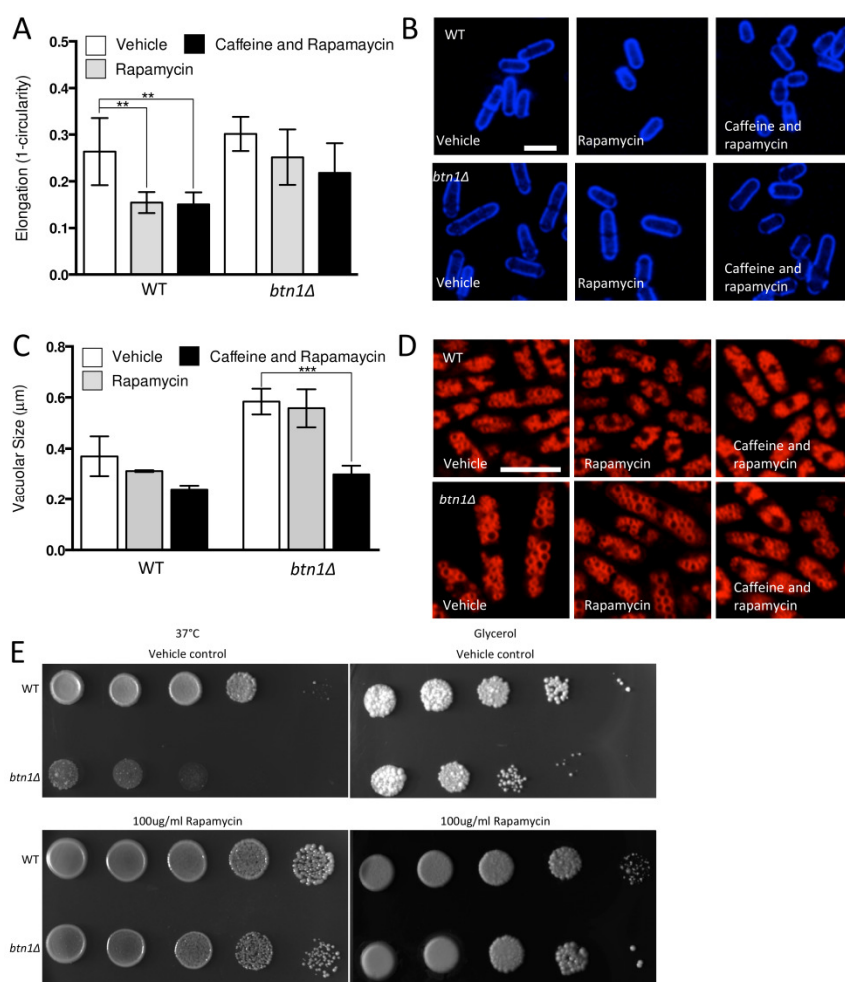


FIGURE 6: Pharmacological inhibition of TORC1 function replicates rescue by overexpression of dominant-negative *rhb1*.

(A) The morphological response of wild-type (WT) and *btn1Δ* cells to the TORC1 antagonists rapamycin (100 $\mu\text{g}/\text{ml}$) and caffeine and rapamycin combined (10 mM and 100 $\mu\text{g}/\text{ml}$ respectively) was analysed following 6 hours in culture using a measure of cell elongation, on a scale of 0 to 1, where 0 represents a perfectly round cell ($1 - \frac{4\pi \text{area}}{\text{perimeter}^2}$). Data shown is a mean (\pm SEM) of 6 independent experiments. Statistical significance between each condition was determined using a one-way ANOVA with a Tukey's multiple comparison post-test (** = $P < 0.01$). **(B)** Representative images of experiments as performed in (A) are shown. Scale bar represents 10 μm . **(C)** Wild-type and *btn1Δ* cells were grown for 6 hours in MM alone or with the TORC1 antagonists rapamycin (100 $\mu\text{g}/\text{ml}$) and caffeine and rapamycin (10 mM and 100 $\mu\text{g}/\text{ml}$ respectively). Vacuole size was then measured in these cells following staining with the vital dye FM4-64. The diameter of 300 vacuoles was measured per data set, and data shown is a mean (\pm SEM) of 4 independent experiments. Statistical analysis was performed using a one-way ANOVA with a Tukey's multiple comparison post-test (***) = $P < 0.001$). **(D)** Representative images of experiments as performed in (C) are shown. Scale bar represents 10 μm . **(E)** WT and *btn1Δ* cells were serially diluted from a log-phase culture (1×10^6

cells/ml) and spotted onto YES plates either containing or lacking rapamycin (100 $\mu\text{g}/\text{ml}$). Plates were then incubated at 37°C for 3-4 days to determine growth at high temperature. They were also spotted onto plates containing glycerol as a carbon source either containing or lacking rapamycin (100 $\mu\text{g}/\text{ml}$). Plates were then incubated at 30°C for 6-7 days to determine growth under non-fermentative conditions. Images are representative of three independent experiments.

in the activity of the connected SAPK pathway, as expression of a constitutively active *wis1* mutant (*wis1DD*) [37] did not rescue these phenotypes (Fig S3A - C). These data confirm that activation of the TORC1 pathway pharmacologically in *btn1Δ* cells rescues most of the phenotypes arising from loss of *btn1* function. However, the pharmacological inhibition of the TORC1 pathway is not completely equivalent to the inhibition of the TORC1 pathway using *dnrhb1* in *btn1Δ* cells.

DISCUSSION

In this study, SGA analysis was used as an unbiased approach to identify the genetic interactors of *btn1*, and place *btn1* into its biological context within the whole cell. This approach highlighted a key role for the Tor kinase complexes, TORC1 and TORC2, in the dysfunctional changes that occur in fission yeast lacking *btn1*, as one third of the interactions connected directly with pathways in which these complexes are active. Further, we have shown that *btn1Δ* cells display defects in their stress response to nitrogen and glucose limitation, in addition to osmoremedial heat sensitivity, consistent with TORC1 and TORC2 dysfunction in these cells (Fig. 7).

Specifically, the SGA identified negative interactions in *tor1*, the core kinase component of TORC2, multiple components of the stress-activated protein kinase (SAPK) pathway, and a component of the linked CWI pathway. In addition, *tco89*, encoding a core component of TORC1, which antagonises both the SAPK cascade and TORC2 signalling, was identified as a positive genetic interactor of *btn1*. *btn1* was also found to interact negatively with a number of genes that display stress-responsive expression.

TORC1 negatively regulates a number of processes associated with cellular catabolism and adaptation to stress [24]. One of these roles is in the repression of autophagy. Autophagy similarly appears important to the fitness of *btn1Δ* cells, as *atg14* and *atg12* were identified as negative interactors of *btn1*, and both are required for autophagosome formation [38]. In support of this work, and the use of yeast as a model, defective autophagy has previously been linked to CLN3 disease [39]. In repressing stress-responsive processes, TORC1 is known to negatively regulate *sty1*, the mitogen-activated protein (MAP) kinase and component of the stress-activated protein kinase (SAPK) cascade [33]. Both *wis4* and *wis1*, encoding the MAP kinase kinase and MAP kinase kinase of the SAPK pathway,

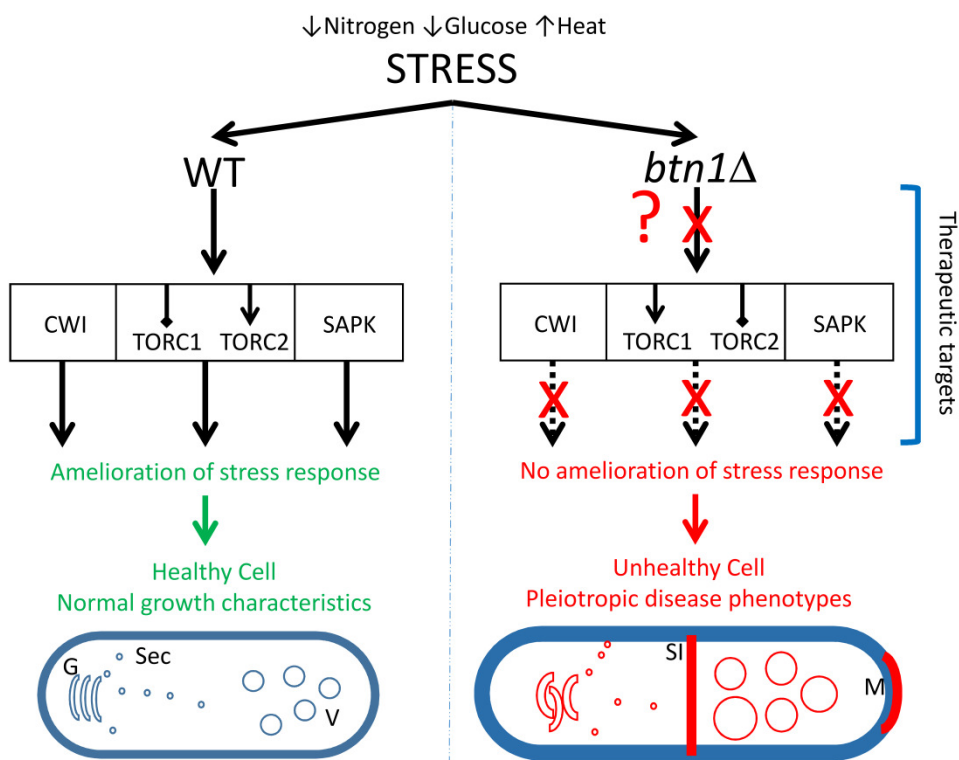


FIGURE 7: Diagrammatic summary of the effect of loss of *btn1* on the response to stress. The left panel shows the response of healthy cells to stresses applied in this study, such as low nitrogen or glucose or raised temperature. These cells are able to respond via interconnected signaling pathways such as CWI, TORC and SAPK. Activation of these pathways allows the cell to respond to the effects of stress and restore cell homeostasis and integrity. In contrast, cells lacking *btn1* are unable to respond to the applied stresses (represented by ‘?’ and ‘X’) and undergo a variety of previously reported responses that include an increase in vacuole size, swollen and disorganized Golgi and mis-trafficking of vacuole enzymes such as carboxypeptidase Y, increased septation index and longer cell cycle and cell length, monopolar growth, defective cell wall, absence of cell rounding (in response to low glucose). Genetic or pharmacological activation of the three signalling pathway provides partial or full rescue of these pleiotropic phenotypes of *btn1Δ* cells. G, Golgi; Sec, secretory vesicles; V, vacuole; SI, division septum; M, monopolar growth.

respectively, interact negatively with *btn1*, as does the transcription factor gene *pap1*, which is a downstream target of *sty1* [40]. Furthermore, *btn1* interacts negatively with a number of genes that display stress-responsive expression.

TORC2 is a positive regulator of stress-responsive processes [29], and is also involved in cytoskeletal organization, vacuolar morphology and glucose sensing [22]. In addition to a negative interaction with the gene encoding the Tor kinase component of TORC2 (*tor1*), *btn1* also negatively interacts with genes encoding components of the connected CWI MAP kinase cascade. The relationship between TORC2 and the CWI pathway is complex. TORC2 is required for the response to cell wall stressors [41], and is a direct regulator of the CWI pathway through the activation of the Rho guanine-nucleotide exchange factor (GEF) ROM2 in budding yeast [42]. In fission yeast, it has recently been shown that Tor1, acting as part of TORC2, enhances Pck2 synthesis to activate the CWI under both cell wall stress and glucose limitation conditions [43].

Despite this positive relationship, recent work in fission yeast has indicated a negative regulation of TORC2 by *pmk1*, the MAP kinase component of the fission yeast CWI pathway, at least in certain conditions [25]. In fission yeast both Rho1 and Rho2 are well established as regulators of the CWI pathway [44, 45]. Rho5 acts as a functional homologue of *rho1*, sharing the role of regulating cell wall homeostasis [46]. More recently, *rho5* has also been shown to be an upstream regulator of the CWI [47]. The regulation of this pathway is complex as Rho1 both positively [45] and negatively [48] regulates the downstream MAP kinase cascade. This potentially intricate relationship is reflected in the interactors of *btn1* that fall within this pathway, that exhibit both positive and negative effects upon signalling. *btn1* exhibits a negative interaction with the *rho1* homologue gene *rho5*, and a number of genes involved in downstream cytoskeletal and polarity components. Despite this, the Rho GEF gene *rgf1*, which is a positive regulator of the CWI pathway [49], is a positive interactor of *btn1* whereas *rdi1* (encoding a GDP dissociation factor) is a negative interactor. This multifaceted pattern of interactions is consistent with current understanding of this pathway, given the complex interactions between these signalling nodes.

Although a process that maintains CWI might seem fungal-specific, and not relevant to disease in a higher eukaryote, previous work in budding yeast revealed similar dysfunctional processes in cells overexpressing α -synuclein as a model for Parkinson's disease, suggesting that there is a mammalian counterpart to the CWI pathway in yeast. Such observations are of specific relevance to CLN3 disease, as α -synuclein is also upregulated in this condition [9]. RHO1 signalling and the CWI pathway are disrupted by overexpression of α -synuclein [50]. Further, it was demonstrated that similar changes in downstream kinase cascades could be observed in mammalian cells overexpressing α -synuclein. Affected kinases included c-Jun, which has previously been linked to CLN3 disease, and is part of a pathway closely related to the SAPK pathway in yeast [51].

This is not the only instance in which Rho signalling has been linked to neurodegeneration. Leucine-rich repeat kinase 2 (LRRK2), mutations in which represent the most common cause of familial late-onset Parkinson's disease, has been shown to bind Rac1, and to a lesser extent RhoA and Cdc42 [52]. All of these binding partners are members of the Rho GTPase family. The binding of LRRK2 to Rac1 led to its activation and relocalisation, and was lost when disease-causing mutations were introduced into LRRK2. Further, the overexpression of Rac1 was shown to be protective in these cells. Other studies have also demonstrated a protective effect of Rho signalling, focusing both on Rho GEFs [53] and the Rho GTPases themselves [54]. Such studies highlight how processes as seemingly specialized as CWI in yeast can be highly informative of processes relevant to disease in higher order eukaryotes. Further, they demonstrate that Rho-dependent signalling could be a vital neuroprotective process in more common neurodegenerative disease, as well as being a key pathway in the neurodegenerative disease model presented in this study.

Importantly, the validation of these interactions during this work revealed interventions that produced a complete rescue of all phenotypes investigated in the *btn1* Δ strain, including phenotypes linked to TORC1 function, TORC2 function, CWI and vacuole homeostasis. Among the interactions investigated, increasing Rho1 levels, and thereby upregulating the main signalling node in the CWI pathway, or repressing TORC1 function (pharmacologically or genetically) led to complete rescues.

More notably, a neuroprotective role of TORC1 repression is already well established in a number of different systems [55]. A protective effect of the TORC1 antagonist rapamycin has been demonstrated in models for Parkinson's disease [57], Huntington's disease [56], spinocerebellar ataxia type 3 [58] and retinal degeneration mediated by mitochondrial dysfunction [59]. In addition, Tor signalling is also elevated in Alzheimer's disease models [60].

It is important to note, however, that targeting TORC1 in disease presents some technical challenges. Although in some studies an increase in lysosome function has been observed upon rapamycin treatment [61], other work indicates that rapamycin is an incomplete antagonist of TORC1 and a poor inducer of lysosomal functions [62], in concert with our observations. Another complication of targeting TORC1 in disease is the antagonistic role of TORC2. TORC2 signalling and the connected CWI pathway were both protective in our model for CLN3 disease. Further to the protective role of Rho signalling in a Parkinson's disease model [50], TORC2/AKT signalling has also been shown to be neuroprotective in a separate study of Parkinson's disease [63]. As a result, general Tor antagonists, such as Torin1, which target both TORC1 and TORC2, do not produce the same positive outcomes that TORC1 specific antagonists are able to elicit [57]. In addition, chronic rapamycin exposure also leads to a reduction in TORC2 activity. This fact could explain why rapamycin has been shown to be detrimental in certain studies, for example in one study using a fruit fly model for Alzheimer's disease [64].

Conclusion

The data presented here highlight a set of interconnected pathways that, when modulated correctly, produce a profound rescue of the dysfunctional changes observed in a yeast model for neurodegeneration caused by mutations in a single gene (Fig. 7). Links between CLN3 and the response to stress have previously been reported in other model organisms [51, 65], supporting the relevance of this yeast work to human CLN3 disease. Importantly however, a link between CLN3 and Tor signalling specifically, as reported here, is a novel mechanistic and therapeutic insight into CLN3 disease, the most common paediatric neurodegenerative disease. Furthermore, the pathways identified display strong parallels with known protective pathways in more common dementias, providing not only strong biological plausibility for the importance of these interactions, but also an indication that common processes may be exploited in therapeutic development for seemingly disparate neurodegenerative diseases.

MATERIALS AND METHODS

Yeast strains and cell growth

The strains used in this study were the wild-type strains SP23 (*h-*, *ura4-D18*, *leu1-32*, *ade6-M210*) and SP38 (*h-*, *ura4-D18*, *leu1-32*, *ade6-210*, *his-*) and *btn1Δ* strains SP29 (*h-*, *btn1::NatMX*, *ura4-D18*, *leu1-32*, *ade6-210*,) and SP35 (*h-*, *btn1::NatMX*, *ura4-D18*, *leu1-32*, *ade6-210*, *his-*). SP29 and SP35 were generated using the long primer method described in [66], using pFA6a-*NatMX* as a template [67]. Both strain backgrounds were used for SGA analysis (two isolates of each) to account for strain background differences, and SP23 and SP29 were used in all other analyses. Cell growth and manipulations were performed as described previously [68]. Minimal media (MM) was used in all experiments, unless otherwise stated. In nitrogen starvation experiments NH₄Cl was omitted. Glucose and glycerol media were made as described previously [69]. Appropriate supplements were added to the media as required. All assays were performed using log-phase cultures (1 × 10⁶ cells/ml). The *dnrhb1* construct (pREP4X-*rhb1*^{DBOK}) was obtained from Dr. Elizabeth Henske [34], and the *gad8* construct (pREP41-*gad8*) from Dr. Ronit Weisman [70]. pREP1-*rho5* was obtained from Dr. Kentaro Nakano [46], pREP41-*rho1* from Dr. Pilar Pérez [48] and pREP1-*wis1DD-3HA6His* from Dr. Kaz Shiozaki [71]. The *GFP-btn1* construct used in this study was described previously (pREP41-*GFP-btn1*) [12]. SP23 containing empty vector (pREP41) was used as a control in all experiments using these constructs.

Synthetic genetic arrays (SGAs)

SGA analysis was performed as described in [20], using a Singer RoToR robot (*S. pombe* settings) and the Bioneer haploid library (v2.0) and analysed as described previously [72]. A control SGA using *ade6::NatMX4* as a query was performed simultaneously. The *ade6Δ* mutant does not alter the fitness of the deletion collection, and arising double mutants are used to determine Bioneer strain fitness and for colony size normalisation. After germination, haploid double mutants were pinned to YES + G418 + Nat in a 1536 format. After three days growth at 30°C, agar plates were imaged using a MultiDoc-It Imaging System (UVP) and processed for analysis using the Gitter image analysis R package [73]. Using Excel, the colony

sizes produced by Gitter were normalized to the median colony size of each plate to account for within-plate positional growth effects and differential plate growth. These normalized values were used to establish the ratio of query *btn1Δ* mutant size to control (*ade6::NatMX4*) colony size. Ratios from the four *btn1Δ* isolates used for the screen were used to calculate a mean ratio. Using this mean value, colony-size ratio scores of < 0.8 were defined as negative interactions, and ratios of > 1.2 as positive interactions. Genetic interactions were scored from two independent biological experiments. Only interactions common to both replicates were considered robust enough for follow-up. Negative and positive interaction sets were tested using PANTHER [74].

Microscopy

All images were obtained using a Leica SPE2 true scanning confocal microscope with 63 × 1.4 NA oil immersion objective. Images were recorded using Leica AF software. Calcofluor-white (Sigma-Aldrich) staining was performed as described previously [68]. Calcofluor-white was used to allow cell segmentation for assays of cell morphology. For assays of cell viability, propidium iodide (Sigma-Aldrich) was added to the cells (15 μg/ml final concentration) at the same point as the calcofluor-white. Staining was performed in a volume of 1 ml, allowed to proceed at room temperature for 10 min, and the cells were washed twice in MM before visualisation. No cell fixation was applied. The vital dye FM4-64 (Molecular Probes) was used to visualise vacuolar morphology. The staining procedure has been described previously [12].

Image analysis

All microscopy image analysis was performed using ImageJ software. For analysis of cell morphology, cells were segmented using the BOA plugin of the quantitative imaging of membrane proteins (Quimp) package [75]. Cell elongation was then determined using the equation: $1 - \left(\frac{4\pi \text{ area}}{\text{perimeter}^2}\right)$. Thirty cells were counted per dataset.

Statistical analysis

All statistical analysis was performed using Prism software, version 6.0C (Graphpad). In instances where only two samples were compared, significance was determined using an unpaired t test. In instances where multiple columns were compared, an ordinary one-way ANOVA was used with a Tukey's multiple-comparison post-test. All error bars represent mean ± standard error of the mean (SEM). In all cases, the statistical test used, p-values and the number of samples analysed are highlighted in the figure legend for clarity.

ACKNOWLEDGMENTS

We would like to thank Dr. Elizabeth Henske, Dr. Ronit Weisman, Prof. Kentaro Nakano, Prof. Pilar Pérez, and Prof. Kaz Shiozaki for generously sharing resources. The research leading to these results (MB, SM) received funding from the European Community's Seventh Framework Programme (FP7/2007- 2013) under Grant Agreement N° 281234 (DEMCHILD), with additional funding from the Batten Disease Family Association, UK, and the Children's Batten Disease Foundation, USA. RB is funded by the University College London (UCL) MRC 4yr Doctoral Training Account in Life and Biomedical Sciences. Research in the Bähler laboratory (CR, JB) is sup-

ported by a BBSRC Research Grant [grant number BB/I012451/1] and a Wellcome Trust Senior Investigator Award [grant number 095598/Z/11/Z].

SUPPLEMENTAL MATERIAL

All supplemental data for this article are available online at www.microbialcell.com.

CONFLICT OF INTEREST

The authors declare no conflict of interest.

REFERENCES

- Jalanko A, Braulke T (2009). Neuronal ceroid lipofuscinoses. *Biochim Biophys Acta* 1793(4): 697-709.
- Williams RE, Mole SE (2012). New nomenclature and classification scheme for the neuronal ceroid lipofuscinoses. *Neurology* 79(2): 183-191.
- Nixon RA, Yang DS, Lee JH (2008). Neurodegenerative lysosomal disorders: a continuum from development to late age. *Autophagy* 4(5): 590-599.
- Brunk UT, Terman A (2002). The mitochondrial-lysosomal axis theory of aging: accumulation of damaged mitochondria as a result of imperfect autophagocytosis. *Eur J Biochem* 269(8): 1996-2002.
- Golabek AA, Kida E, Walus M, Kaczmarek W, Michalewski M, Wisniewski KE (2000). CLN3 protein regulates lysosomal pH and alters intracellular processing of Alzheimer's amyloid-beta protein precursor and cathepsin D in human cells. *Mol Genet Metab* 70(3): 203-213.
- Holopainen JM, Saarikoski J, Kinnunen PK, Jarvela I (2001). Elevated lysosomal pH in neuronal ceroid lipofuscinoses (NCLs). *Eur J Biochem* 268(22): 5851-5856.
- Luiro K, Kopra O, Blom T, Gentile M, Mitchison HM, Hovatta I, Tornquist K, Jalanko A (2006). Batten disease (JNCL) is linked to disturbances in mitochondrial, cytoskeletal, and synaptic compartments. *J Neurosci Res* 84(5): 1124-1138.
- Glenner GG (1988). Alzheimer's disease: its proteins and genes. *Cell* 52(3): 307-308.
- Kang S, Heo TH, Kim SJ (2014). Altered levels of alpha-synuclein and sphingolipids in Batten disease lymphoblast cells. *Gene* 539(2): 181-185.
- Nussbaum RL, Polymeropoulos MH (1997). Genetics of Parkinson's disease. *Hum Mol Genet* 6(10): 1687-1691.
- Bond M, Holthaus SM, Tammen I, Tear G, Russell C (2013). Use of model organisms for the study of neuronal ceroid lipofuscinosis. *Biochim Biophys Acta* 1832(11): 1842-1865.
- Gachet Y, Codlin S, Hyams JS, Mole SE (2005). *btn1*, the fission yeast homologue of the human Batten disease gene, *CLN3*, regulates vacuole homeostasis. *J Cell Sci* 118(23): 5525-5536.
- Codlin S, Mole SE (2009). *btn1*, the fission yeast orthologue of *CLN3*, is required for Golgi exit of Vps10 and vacuole protein sorting. *J Cell Sci* 122(8): 1163-1173.
- Kitzmüller C, Haines R, Codlin S, Cutler DF, Mole SE (2008). A function retained by the common mutant *CLN3* protein is responsible for the late onset of juvenile neuronal ceroid lipofuscinosis (JNCL). *Hum Mol Genet* 17(2): 303-312.

COPYRIGHT

© 2015 Bond *et al.* This is an open-access article released under the terms of the Creative Commons Attribution (CC BY) license, which allows the unrestricted use, distribution, and reproduction in any medium, provided the original author and source are acknowledged.

Please cite this article as: Michael E. Bond, Rachel Brown, Charalampos Rallis, Jürg Bähler and Sara E. Mole (2015). A central role for TOR signalling in a yeast model for juvenile CLN3 disease. *Microbial Cell* 2(12): 466-480. doi: 10.15698/mic2015.12.241

15. Codlin S, Haines RL, Mole SE (2008). *btn1* affects endocytosis, polarisation of sterol-rich membrane domains and polarised growth in *Schizosaccharomyces pombe*. *Traffic* 9(6): 936-950.

16. Codlin S, Haines RL, Burden JJE, Mole SE (2008). *btn1* affects cytokinesis and cell-wall deposition by independent mechanisms, one of which is linked to dysregulation of vacuole pH. *J Cell Sci* 121(17): 2860-2870.

17. Pears MR, Codlin S, Haines RL, White IJ, Mortishire-Smith RJ, Mole SE, Griffin JL (2010). Deletion of *btn1*, an orthologue of *CLN3*, increases glycolysis and perturbs amino acid metabolism in the fission yeast model of Batten disease. *Molecular bioSystems* 6(6): 1093-1102.

18. Luiro K, Yliannala K, Ahtiainen L, Maunu H, Jarvela I, Kytälä A, Jalanko A (2004). Interconnections of *CLN3*, *Hook1* and *Rab* proteins link Batten disease to defects in the endocytic pathway. *Hum Mol Genet* 13(23): 3017-3027.

19. Metcalfe DJ, Calvi AA, Seamann MNJ, Mitchison HM, Cutler DF (2008). Loss of the Batten disease gene *CLN3* prevents exit from the TGN of the mannose 6-phosphate receptor. *Traffic* 11(11): 1905-1914.

20. Baryshnikova A, Costanzo M, Dixon S, Vizeacoumar FJ, Myers CL, Andrews B, Boone C (2010). Synthetic genetic array (SGA) analysis in *Saccharomyces cerevisiae* and *Schizosaccharomyces pombe*. *Methods Enzymol* 470:145-179.

21. Willingham S, Outeiro TF, DeVit MJ, Lindquist SL, Muchowski PJ (2003). Yeast genes that enhance the toxicity of a mutant huntingtin fragment or alpha-synuclein. *Science* 302(5651): 1769-1772.

22. Ikai N, Nakazawa N, Hayashi T, Yanagida M (2011). The reverse, but coordinated, roles of Tor2 (TORC1) and Tor1 (TORC2) kinases for growth, cell cycle and separase-mediated mitosis in *Schizosaccharomyces pombe*. *Biol Open* 1(3): 110007.

23. Weisman R, Roitburg I, Schonbrun M, Harari R, Kupiec M (2007). Opposite effects of *tor1* and *tor2* on nitrogen starvation responses in fission yeast. *Genetics* 175(3): 1153-1162.

24. Matsuo T, Otsubo Y, Urano J, Tamanoi F, Yamamoto M (2007). Loss of the TOR kinase *Tor2* mimics nitrogen starvation and activates the sexual development pathway in fission yeast. *Molecular and cellular biology* 27(8): 3154-3164.

25. Cohen A, Kupiec M, Weisman R (2014). Glucose activates TORC2-Gad8 protein via positive regulation of the cAMP/cAMP-dependent protein kinase A (PKA) pathway and negative regulation of the Pmk1 protein-mitogen-activated protein kinase pathway. *J Biol Chem* 289(31): 21727-21737.

26. Ikeda K, Morigasaki S, Tatebe H, Tamanoi F, Shiozaki K (2008). Fission yeast TOR complex 2 activates the AGC-family Gad8 kinase essential for stress resistance and cell cycle control. *Cell cycle* 7(3): 358-364.
27. Hanyu Y, Imai KK, Kawasaki Y, Nakamura T, Nakaseko Y, Nagao K, Kokubu A, Ebe M, Fujisawa A, Hayashi T, Obuse C, Yanagida M (2009). Schizosaccharomyces pombe cell division cycle under limited glucose requires Ssp1 kinase, the putative CaMKK, and Sds23, a PP2A-related phosphatase inhibitor. *Genes Cells* 14(5): 539-554.
28. Levin DE (2005). Cell wall integrity signaling in Saccharomyces cerevisiae. *Microbiol Mol Biol Rev* 69(2): 262-291.
29. Matsuo T, Kubo Y, Watanabe Y, Yamamoto M (2003). Schizosaccharomyces pombe AGC family kinase Gad8p forms a conserved signaling module with TOR and PDK1-like kinases. *EMBO* 22(12): 3073-3083.
30. Madrid M, Fernandez-Zapata J, Sanchez-Mir L, Soto T, Franco A, Vicente-Soler J, Gacto M, Cansado J (2013). Role of the fission yeast cell integrity MAPK pathway in response to glucose limitation. *BMC Microbiol* 13:34.
31. Sugiura R, Toda T, Shuntoh H, Yanagida M, Kuno T (1998). pmp1+, a suppressor of calcineurin deficiency, encodes a novel MAP kinase phosphatase in fission yeast. *EMBO J* 17(1): 140-148.
32. Mutoh T, Nakano K, Mabuchi I (2005). Rho1-GEFs Rgf1 and Rgf2 are involved in formation of cell wall and septum, while Rgf3 is involved in cytokinesis in fission yeast. *Genes Cells* 10(12): 1189-1202.
33. Hartmuth S, Petersen J (2009). Fission yeast Tor1 functions as part of TORC1 to control mitotic entry through the stress MAPK pathway following nutrient stress. *J Cell Sci* 122(Pt 11): 1737-1746.
34. van Slegtenhorst M, Carr E, Stoyanova R, Kruger WD, Henske EP (2004). Tsc1+ and tsc2+ regulate arginine uptake and metabolism in Schizosaccharomyces pombe. *J Biol Chem* 279(13): 12706-12713.
35. Rallis C, Codlin S, Bahler J (2013). TORC1 signaling inhibition by rapamycin and caffeine affect lifespan, global gene expression, and cell proliferation of fission yeast. *Aging Cell* 12(4): 563-573.
36. Nakashima A, Sato T, Tamanoi F (2010). Fission yeast TORC1 regulates phosphorylation of ribosomal S6 proteins in response to nutrients and its activity is inhibited by rapamycin. *J Cell Sci* 123(5): 777-786.
37. Nguyen AN, Shiozaki K (1999). Heat-shock-induced activation of stress MAP kinase is regulated by threonine- and tyrosine-specific phosphatases. *Genes & development* 13(13): 1653-1663.
38. Mukaiyama H, Nakase M, Nakamura T, Kakinuma Y, Takegawa K (2010). Autophagy in the fission yeast Schizosaccharomyces pombe. *FEBS Lett* 584(7): 1327-1334.
39. Chandrachud U, Walker MW, Simas AM, Heetveld S, Petcherski A, Klein M, Oh H, Wolf P, Zhao WN, Norton S, Haggarty SJ, Lloyd-Evans E, Cotman SL (2015). Unbiased Cell-based Screening in a Neuronal Cell Model of Batten Disease Highlights an Interaction between Ca2+ Homeostasis, Autophagy, and CLN3 Protein Function. *J Biol Chem* 290(23): 14361-14380.
40. Toone WM, Kuge S, Samuels M, Morgan BA, Toda T, Jones N (1998). Regulation of the fission yeast transcription factor Pap1 by oxidative stress: requirement for the nuclear export factor Crm1 (Exportin) and the stress-activated MAP kinase Sty1/Spc1. *Genes & development* 12(10): 1453-1463.
41. Halova L, Du W, Kirkham S, Smith DL, Petersen J (2013). Phosphorylation of the TOR ATP binding domain by AGC kinase constitutes a novel mode of TOR inhibition. *J Cell Biol* 203(4): 595-604.
42. Schmidt A, Bickle M, Beck T, Hall MN (1997). The yeast phosphatidylinositol kinase homolog TOR2 activates RHO1 and RHO2 via the exchange factor ROM2. *Cell* 88(4): 531-542.
43. Madrid M, Jiménez R, Sánchez-Mir L, Soto T, Franco A, Vicente-Soler J, Gacto M, Pérez P, Cansado J (2015). Multiple layers of regulation influence cell integrity control by the PKC ortholog Pck2 in fission yeast. *J Cell Sci* 128(2): 266-80.
44. Sanchez-Mir L, Franco A, Martín-García R, Madrid M, Vicente-Soler J, Soto T, Gacto M, Perez P, Cansado J (2014). Rho2 palmitoylation is required for plasma membrane localization and proper signaling to the fission yeast cell integrity mitogen-activated protein kinase pathway. *Mol Cell Biol* 34(14): 2745-2759.
45. Sanchez-Mir L, Soto T, Franco A, Madrid M, Viana RA, Vicente J, Gacto M, Perez P, Cansado J (2014). Rho1 GTPase and PKC ortholog Pck1 are upstream activators of the cell integrity MAPK pathway in fission yeast. *PLoS One* 9(1): e88020.
46. Nakano K, Arai R, Mabuchi I (2005). Small GTPase Rho5 is a functional homologue of Rho1, which controls cell shape and septation in fission yeast. *FEBS Lett* 579(23): 5181-5186.
47. Doi A, Kita A, Kanda Y, Uno T, Asami K, Satoh R, Nakano K, Sugiura R (2015). Geranylgeranyltransferase Cwg2-Rho4/Rho5 module is implicated in the Pmk1 MAP kinase-mediated cell wall integrity pathway in fission yeast. *Genes Cells* 20(4): 310-323.
48. Viana RA, Pinar M, Soto T, Coll PM, Cansado J, Perez P (2013). Negative functional interaction between cell integrity MAPK pathway and Rho1 GTPase in fission yeast. *Genetics* 195(2): 421-432.
49. Garcia P, Tajadura V, Sanchez Y (2009). The Rho1p exchange factor Rgf1p signals upstream from the Pmk1 mitogen-activated protein kinase pathway in fission yeast. *Mol Biol Cell* 20(2): 721-731.
50. Wang S, Xu B, Liou LC, Ren Q, Huang S, Luo Y, Zhang Z, Witt SN (2012). alpha-Synuclein disrupts stress signaling by inhibiting polo-like kinase Cdc5/Plk2. *Proc Natl Acad Sci USA* 109(40): 16119-16124.
51. Tuxworth RI, Vivancos V, O'Hare MB, Tear G (2009). Interactions between the juvenile Batten disease gene, CLN3, and the Notch and JNK signalling pathways. *Hum Mol Genet* 18(4): 667-678.
52. Chan D, Citro A, Cordy JM, Shen GC, Wolozin B (2011). Rac1 protein rescues neurite retraction caused by G2019S leucine-rich repeat kinase 2 (LRRK2). *J Biol Chem* 286(18): 16140-16149.
53. Namekata K, Harada C, Taya C, Guo X, Kimura H, Parada LF, Harada T (2010). Dock3 induces axonal outgrowth by stimulating membrane recruitment of the WAVE complex. *Proc Natl Acad Sci U S A* 107(16): 7586-7591.
54. Mocholi E, Ballester-Lurbe B, Arque G, Poch E, Peris B, Guerri C, Dierssen M, Guasch RM, Terrado J, Perez-Roger I (2011). RhoE deficiency produces postnatal lethality, profound motor deficits and neurodevelopmental delay in mice. *PLoS One* 6(4): e19236.
55. Bove J, Martínez-Vicente M, Vila M (2011). Fighting neurodegeneration with rapamycin: mechanistic insights. *Nat Rev Neurosci* 12(8): 437-452.
56. Sarkar S, Ravikumar B, Floto RA, Rubinsztein DC (2009). Rapamycin and mTOR-independent autophagy inducers ameliorate toxicity of polyglutamine-expanded huntingtin and related proteinopathies. *Cell death and differentiation* 16(1): 46-56.
57. Malagelada C, Jin ZH, Jackson-Lewis V, Przedborski S, Greene LA (2010). Rapamycin protects against neuron death in in vitro and in vivo models of Parkinson's disease. *J Neurosci* 30(3): 1166-1175.
58. Menzies FM, Huebener J, Renna M, Bonin M, Riess O, Rubinsztein DC (2010). Autophagy induction reduces mutant ataxin-3 levels and toxicity in a mouse model of spinocerebellar ataxia type 3. *Brain* 133(Pt 1): 93-104.

59. Zhao C, Yasumura D, Li X, Matthes M, Lloyd M, Nielsen G, Ahern K, Snyder M, Bok D, Dunaief JL, LaVail MM, Vollrath D (2011). mTOR-mediated dedifferentiation of the retinal pigment epithelium initiates photoreceptor degeneration in mice. **J Clin Invest** 121(1): 369-383.
60. Caccamo A, Maldonado MA, Majumder S, Medina DX, Holbein W, Magri A, Oddo S (2011). Naturally secreted amyloid-beta increases mammalian target of rapamycin (mTOR) activity via a PRAS40-mediated mechanism. **J Biol Chem** 286(11): 8924-8932.
61. Dehay B, Bove J, Rodriguez-Muela N, Perier C, Recasens A, Boya P, Vila M (2010). Pathogenic lysosomal depletion in Parkinson's disease. **J Neurosci** 30(37): 12535-12544.
62. Zhou J, Tan SH, Nicolas V, Bauvy C, Yang ND, Zhang J, Xue Y, Codogno P, Shen HM (2013). Activation of lysosomal function in the course of autophagy via mTORC1 suppression and autophagosome-lysosome fusion. **Cell Res** 23(4): 508-523.
63. Ries V, Henchcliffe C, Kareva T, Rzhetskaya M, Bland R, During MJ, Kholodilov N, Burke RE (2006). Oncoprotein Akt/PKB induces trophic effects in murine models of Parkinson's disease. **Proc Natl Acad Sci U S A** 103(49): 18757-18762.
64. Ling D, Song HJ, Garza D, Neufeld TP, Salvaterra PM (2009). Abeta42-induced neurodegeneration via an age-dependent autophagic-lysosomal injury in *Drosophila*. **PLoS One** 4(1): e4201.
65. Tuxworth RI, Chen H, Vivancos V, Carvajal N, Huang X, Tear G (2011). The Batten disease gene CLN3 is required for the response to oxidative stress. **Hum Mol Genet** 20(10): 2037-2047.
66. Bahler J, Wu JQ, Longtine MS, Shah NG, McKenzie A, 3rd, Steever AB, Wach A, Philippsen P, Pringle JR (1998). Heterologous modules for efficient and versatile PCR-based gene targeting in *Schizosaccharomyces pombe*. **Yeast** 14(10): 943-951.
67. Sato M, Dhut S, Toda T (2005). New drug-resistant cassettes for gene disruption and epitope tagging in *Schizosaccharomyces pombe*. **Yeast** 22(7): 583-591.
68. Moreno S, Klar A, Nurse P (1991). Molecular genetic analysis of fission yeast *Schizosaccharomyces pombe*. **Methods Enzymol** 194:795-823.
69. Rorbach J, Richter R, Wessels HJ, Wydro M, Pekalski M, Farhoud M, Kuhl I, Gaisne M, Bonnefoy N, Smeitink JA, Lightowlers RN, Chrzanoska-Lightowlers ZM (2008). The human mitochondrial ribosome recycling factor is essential for cell viability. **Nucleic Acids Res** 36(18): 5787-5799.
70. Schonbrun M, Laor D, Lopez-Maury L, Bahler J, Kupiec M, Weisman R (2009). TOR complex 2 controls gene silencing, telomere length maintenance, and survival under DNA-damaging conditions. **Mol Cell Biol** 29(16): 4584-4594.
71. Tatebe H, Shiozaki K (2003). Identification of Cdc37 as a novel regulator of the stress-responsive mitogen-activated protein kinase. **Mol Cell Biol** 23(15): 5132-5142.
72. Rallis C, Lopez-Maury L, Georgescu T, Pancaldi V, Bahler J (2014). Systematic screen for mutants resistant to TORC1 inhibition in fission yeast reveals genes involved in cellular ageing and growth. **Biol Open** 3(2): 161-171.
73. Wagih O, Parts L (2014). gitter: a robust and accurate method for quantification of colony sizes from plate images. **G3 (Bethesda)** 4(3): 547-552.
74. Mi H, Muruganujan A, Thomas PD (2013). PANTHER in 2013: modeling the evolution of gene function, and other gene attributes, in the context of phylogenetic trees. **Nucleic Acids Res** 41(Database issue): D377-386.
75. Bosgraaf L, van Haastert PJ, Bretschneider T (2009). Analysis of cell movement by simultaneous quantification of local membrane displacement and fluorescent intensities using Quimp2. **Cell Motil Cytoskeleton** 66(3): 156-165.
76. Chen D, Toone WM, Mata J, Lyne R, Burns G, Kivinen K, Brazma A, Jones N, Bahler J (2003). Global transcriptional responses of fission yeast to environmental stress. **Mol Biol Cell** 14(1): 214-229.